MULTISCALE EDGE DETECTION AND GRADIENT VECTOR FLOW SNAKES FOR AUTOMATED IDENTIFICATION OF THE CAROTID ARTERY WALL IN LONGITUDINAL B-MODE ULTRASOUND IMAGES

A.I. Matsakou[1], N.Tsiaparas[1], S.Golemati[2] and K.S.Nikita[1]

[1]Biomedical Simulations & Imaging Laboratory, National Technical University of Athens, Athens, Greece
[2]First Intensive Care Unit, Medical School, National & Kapodistrian University of Athens, Athens, Greece

ABSTRACT

This paper proposes a fully automatic active-contour-based segmentation method, for the detection of the carotid artery wall in longitudinal B-mode images. A multiscale edge detection methodology is used for the definition of an initial snake contour, followed by a gradient vector flow (GVF) snake. The multiscale edge detection method is based on finding the local maxima of the wavelet transform of the image, which is very close to the real contour. The GVF snake is based on the calculation of the image edge map and the calculation of the GVF field which guides the deformation for the estimation of the real arterial wall boundaries. In twenty cases of healthy carotid arteries the sensitivity, specificity and accuracy were higher than 0.97, 0.99 and 0.98 respectively, for both diastolic and systolic cases. In conclusion, the proposed methodology provides a new accurate procedure to detect the arterial wall in ultrasound images of the carotid artery.

Index Terms— Ultrasound imaging, Carotid artery, Multi-scale edge detection, Wavelet transform, Gradient vector flow snake

1. INTRODUCTION

B-mode ultrasound imaging of the carotid artery is widely used for the assessment of the morphology of the arterial wall and the diagnosis of atherosclerosis. Measurements of lumen diameter are often used for the estimation of arterial elasticity [1]. These measurements are conventionally obtained directly from the image by manually tracing the wall-lumen interfaces for both the anterior and posterior arterial walls. This procedure is not only time-consuming but also extremely subjective because it depends on the training, the experience and the expertise of the observer. Therefore the manual measurements suffer from inter- and intra-observer variability [2].

The majority of the methods for the segmentation of longitudinal images of the carotid artery wall are semiautomatic due to user interaction for the selection of the region of interest (ROI) of the image or/and the initialization step. Previous attempts to implement completely automated segmentation include the application of the Hough transform (HT) [3], HT-initialized active contours [4], combination of dynamic programming and cubic spline [5] and edge flow models based on directional probability maps using intensity and texture features [6]. User-independent integrated approaches have also been developed [7][8].

In an attempt to further improve the automatic detection of the random-shaped arterial wall in ultrasound images, a multiscale approach is considered. Such approach may be beneficial to ultrasound images, which suffer from speckle noise, assuming that speckle is not found in all scales. Specifically, the wavelet transform (WT), which allows for the decomposition of images into their elementary constituents across scales, can be used to define edges in multiple scales. Hence, the contour of small structures as well as the boundaries of larger objects can be detected. Due to its multiscale nature, WT has the ability to detect edges even in high background noise. WT-based methodologies have proven beneficial for texture analysis of ultrasound images of carotid plaque [9]. In image segmentation, a wavelet-based multiscale edge detector has been used to compute edges in a certain length and intensity range of images and efficiently extract pulmonary nodules' boundaries in chest radiographs [10].

The purpose of this paper was to investigate the possibility of using a wavelet-based multiscale edge detection technique to initialize a gradient vector flow (GVF) snake, in an attempt to accurately detect the carotid artery wall. The results of the method were validated by means of receiver operating characteristic (ROC) analysis in real ultrasound images through comparisons with manually delineated wall boundaries.

2. MATERIAL AND METHODS

2.1. Recording of Ultrasound Images

A total of 10 systolic and 10 diastolic B-mode longitudinal ultrasound images were selected from image sequences of the common carotid artery. The images were recorded from young subjects (ages: 25-32 years) with normal (non-stenotic) carotid arteries. For each subject, image sequences were acquired by an ATL (Advanced Technology Laboratory) Ultramark 4 Duplex scanner (Philips Medical Systems, Bothell, WA, USA) and a high resolution 7.5MHz linear array scan head. Scanner settings were constant for all measurements at the following values: dynamic range 60dB; 2-D gray map linear; persistence low; frame rate high. The sequences were recorded at a rate of 25 frames/s for approximately 3 seconds (2-3 cardiac cycles) during breath holding. Images were normalized so that the average gray-scale median (GSM) of the pixels in the blood ranged between 0 and 5, whereas that of the adventitia between 180 and 190 according to widely accepted specifications.

2.2. Detection of Arterial Wall Boundaries

The proposed method is composed of three main stages. The first stage is the automatic selection of the ROI, i.e the image area containing the common carotid artery, using the methodology described in [3]. Briefly, the ROI selection consists of morphological opening, thresholding and detection of the first and last non-zero lines and columns, which define the cropping

boundaries. This stage is very important because it minimizes the possibility to detect unwanted structures and reduces the computational cost of the segmentation. The second stage is the initialization of the arterial wall contour using wavelet-based multiscale edge detection and the third stage is the refinement of the initial contour using open GVF snakes. The following sections describe the second and third stages of the proposed methodology in detail.

2.2.1. Wavelet-based multiscale edge detection

The discrete wavelet transform (DWT) of a signal is defined as its inner product with a family of functions $\varphi_{j,k}(t) = 2^{j/2}\varphi(2^j t - k)$ and $\psi_{j,k}(t) = 2^{j/2}\psi(2^j t - k)$, consisting of versions of the prototype scaling $\varphi(t)$ and wavelet $\psi(t)$ functions, discretized at scale j and at translation k. For images, the 2D DWT consists of a DWT on the rows of the image and a DWT on the columns of the resulting image. The result of each DWT is followed by downsampling on the columns and rows, respectively. The decomposition of the image yields an approximation subimage Ap and three detail subimages (horizontal H, vertical V and diagonal D) for every scale j. To ensure good edge localization for the edge detection, the 2D overcomplete DWT (ODWT) should be used. It is similar to the 2D DWT, but no downsampling is performed.

The wavelet-based multiscale edge detection algorithm consists of the following steps:

1) Smoothing of the selected ROI image using a symmetric Gaussian low-pass filter and morphological closing [3].

2) Computation of the 2D ODWT of the ROI image at scales 1:j.

3) Computation of the modulus M_j and the angle A_j, given by:

$$M_j = \sqrt{(H_j)^2 + (V_j)^2}$$
$$A_j = \begin{cases} a_j & , H_j \geq 0 \\ \pi - a_j & , H_j < 0 \end{cases} \qquad (1)$$

where $a_j = \tan^{-1}\left(V_j / H_j\right)$.

4) Detection of the points (edges) $\tilde{H}(u_{j,p})$ and $\tilde{V}(u_{j,p})$ of the modulus subimages that are larger than the two neighbors whose positions are in the direction indicated by the angle value A_j at the corresponding location. At every scale, edges are defined as points where the modulus of the gradient vector is maximum in the direction towards which the gradient vector points in the subimage plane [11].

5) Reconstruction of the image, using only $\tilde{H}_j$ and $\tilde{V}_j$ from each scale. Approximation subimages can be ignored because they contain the low frequency content, whereas edges correspond to high frequencies in the image. According to [11], the diagonal subimages can also be disregarded and the reconstructed image still remains visually indistinguishable from the original.

6) Thresholding of the reconstructed image using the threshold $T = mean + 2 * std$, where *mean* is the mean intensity and *std* is the standard deviation of the intensities of the reconstructed image.

At the end of the algorithm the reconstructed image of edges is post-processed. Due to the reconstruction procedure, the edges in the image are thick; therefore morphological thinning of the binary edge image is performed. Furthermore the edges of the anterior and the posterior walls are identified according to intensity gradients along the image, as the first edge segments above and below the center of the lumen. Finally, unconnected edge segments with length less than 3 pixels are removed and the remaining edge segments are linked, using linear interpolation.

2.2.2. GVF-based methodology

In this last stage of the proposed method, the arterial contour defined in the previous stage is used as an initial contour for the active-contour-based methodology. An open GVF snake is implemented through the following three distinct steps:

1) Calculation of the image edge map. The first step of the snake-based methodology includes processing of the reduced image, which resulted from the ROI selection stage, in order to estimate the gradient field of the image edge map. This step includes the following tasks: (a) calculation of the gradient field by applying the gradient operator, (b) thresholding the gradient field to remove the small gradient values due to speckle noise and to enhance the strong edges, (c) morphological closing and opening of the image and smoothing of the gradient field, using a symmetric Gaussian low-pass filter, and (d) gradient operator application to estimate the image edge map. The edge map derived from the image has large values near the edges and zero value in homogeneous regions of the image.

2) Calculation of the GVF field. In this step, the GVF field, defined by $\mathbf{v}(x,y) = [u(x,y), v(x,y)]$, was calculated by minimizing the energy functional [12]:

$$E = \iint \mu \cdot (u_x^2 + u_y^2 + v_x^2 + v_y^2) + \left|\nabla f\right|^2 \left|\mathbf{v} - \nabla f\right|^2 dxdy \qquad (2)$$

where f is the image edge map, calculated in the previous step, $\nabla f = (f_x, f_y)$ is the gradient of the image edge map, and μ is a regularization parameter that should be set according to the amount of noise present in the image (more noise, increased μ) [12]. A value of 0.2 was used for μ in this study.

Minimizing the energy functional of equation (2) gives rise to the following two independent Euler equations [12]:

$$\mu\nabla^2 u - (u - f_x)(f_x^2 + f_y^2) = 0$$
$$\mu\nabla^2 v - (v - f_y)(f_x^2 + f_y^2) = 0 \qquad (3)$$

where ∇^2 is the Laplacian operator. The GVF field can be found solving equations (3).

3) Deformation of the initial contour based on the GVF field. Finally, the initial contour defined in the initialization stage is considered to be a snake that uses the GVF field as its external force. This GVF snake is defined as the parametric curve $\mathbf{x}(s) = [x(s), y(s)]$ solving the dynamic equation [12]:

$$\mathbf{x}_t(s,t) = \alpha \cdot \mathbf{x}'' - \beta \cdot \mathbf{x}'''' + k \cdot \mathbf{v}(\mathbf{x}) \qquad (4)$$

where $\mathbf{x}$ is treated as a function of time t and space s, α and β are the tension and rigidity parameters of the snake, respectively, and k is a parameter that controls the extent to which the GVF field affects the deformation of the curve. The values $\alpha = 0.05$, $\beta = 0$, and $k=1$ were used in this study.

The dynamic equation (4) is solved by discretization and iteration, in identical fashion to the traditional snake. The iterative equations for the snake deformation of the initial curve are [12]:

$$\mathbf{x}_t = (\mathbf{A} + \gamma \cdot \mathbf{I})^{-1}(\gamma \cdot \mathbf{x}_{t-1} + k \cdot \mathbf{u}(\mathbf{x}_{t-1}, \mathbf{y}_{t-1}))$$
$$\mathbf{y}_t = (\mathbf{A} + \gamma \cdot \mathbf{I})^{-1}(\gamma \cdot \mathbf{y}_{t-1} + k \cdot \mathbf{u}(\mathbf{x}_{t-1}, \mathbf{y}_{t-1})) \qquad (5)$$

Where **x** and **y** are the coordinates' vectors of the points of the curve, $\gamma = 1/\Delta t$ the step size of the iteration, **I** a diagonal identity matrix and **A** is a pentadiagonal matrix with incorporated boundary conditions for the open-ended snake used for the longitudinal images. After each iteration, the snake is dynamically re-parameterized to maintain point separation within 0.5-1.5 pixels [13].

2.3. Validation

To evaluate the performance of the proposed method, the automatically detected wall-lumen boundaries were compared with the boundaries defined manually by an expert physician. The area corresponding to automatic segmentation is the surface defined by the two random-shaped boundaries corresponding to the anterior and posterior walls (calculated from the deformation of the snake) and the two lines connecting the previous ones at the left and right edges. The area corresponding to the manual segmentation is the surface defined by the two random-shaped boundaries corresponding to the anterior and posterior walls (delineated by the physician) and the two lines connecting their left and right edges.

ROC analysis was used to assess the sensitivity, specificity, and accuracy of the method calculated as described in [3], after estimating the number of true positive, true negative, false positive and false negative pixels, for the images corresponding to diastole and systole. True positive pixels are the pixels that automatic and manual segmentation identified as segmented; true negative are the pixels that automatic and manual segmentation did not identify as segmented; false positive are the pixels that automatic segmentation identified as segmented, but manual segmentation did not; and false negative pixels are the pixels that manual segmentation identified as segmented but automatic segmentation did not.

3. RESULTS

In this study, four scales of 2D ODWT decomposition were implemented using Haar as the wavelet function. Figure 1 shows the horizontal H_j, the vertical V_j, the modulus M_j and the angle A_j subimages as well as the edges E_j, for scales 1 and 2. Edge points in E_2 with high modulus values in M_2 correspond to sharper intensity variations of the image, and therefore are more likely to correspond to actual edges. On the other hand, edge points in E_1 with lower modulus values in M_1 are less likely to correspond to actual edges; they may be due to noise.

In Figure 2 an application of each step of the proposed method is presented, in a somewhat noisy image of a longitudinal section of the carotid artery. Although the edges in Fig.2(d) seem very close to the ideal ones, in many cases this result does not correspond to the desired boundaries, because it is composed of linked horizontal edge segments; therefore the steps following (d) should be implemented for all cases.

Table 1 shows the ROC analysis results for the sensitivity, specificity and accuracy (average values $\pm$ std) of the suggested method. As we can see, all indices were particularly high for both systole and diastole.

The mean computational time for the detection of the anterior and posterior wall boundaries in one image did not exceed 50s using MATLAB R2009a (The MathWorks Inc., Natick, USA) on a dual 3.00GHz personal computer.

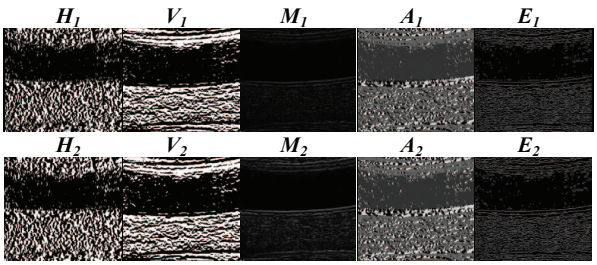


Fig.1 Examples of wavelet-based multiscale edge detection subimages for two scales. *H*, *V*, *M* and *A* are the horizontal, vertical, modulus and angle subimages, respectively, whereas *E* represents the edges of the corresponding scale.

4. DISCUSSION

The proposed methodology provides a fully automated identification of the arterial lumen in B-mode longitudinal ultrasound images. The application of the methodology on images from healthy subjects is a first step in an attempt to automate the diagnostic procedure for carotid atherosclerosis. The main advantage of the method is the wavelet-based multiscale edge detection step, which contributes to the snake initialization, and detects the lumen boundaries, even in the presence of noise.

The ability of the wavelet decomposition to detect structures in an image can be seen in Figure 1. The horizontal subimages represent trends along columns of the image, whereas vertical subimages represent trends along rows of the image. In the modulus subimages at scale 2 the intima-media-complex (IMC) of the posterior wall can be identified, thus indicating the possibility of using the methodology for its detection and the measurement of the intima-media-thickness (IMT).

Compared to previous similar works, the suggested methodology produced generally better results. Molinari *et al*. [6][8] reported an overall Figure of Merit (FoM) equal to 94.8% and 84.7% respectively, for automated techniques based on edge flow models, and intensity local statistics combined with line fitting and fuzzy classification. Delsanto *et al*. [7] also detected the intimal and advential layers of the carotid wall using a gradient-based segmentation method combined with snakes and fuzzy K-means, with an overall FoM equal to 91.5%. It is pointed out, however, that direct comparison with these studies is not straightforward, because the image samples and validation criteria are different.

The HT-initialized snakes [4] already had particularly high performances, with sensitivity, specificity and accuracy reaching 0.97, 0.99 and 0.98, respectively, for both the diastolic and systolic cases on the same image dataset. Wavelet-based snakes slightly improved these findings.

The performance of the methodology can be affected by the parameter values used in the image edge map calculation step. Therefore these values should be carefully selected according to the image characteristics. In this paper, the values used were based on experiments performed on a small set of data, which was not used in the validation process. For a globally optimal set of parameters, an optimization on a large image dataset is critical. The snake parameters α and β were selected according to previously reported values [14]. The low value of α allows the snake's points to change their spacing without forming discontinuities, whereas

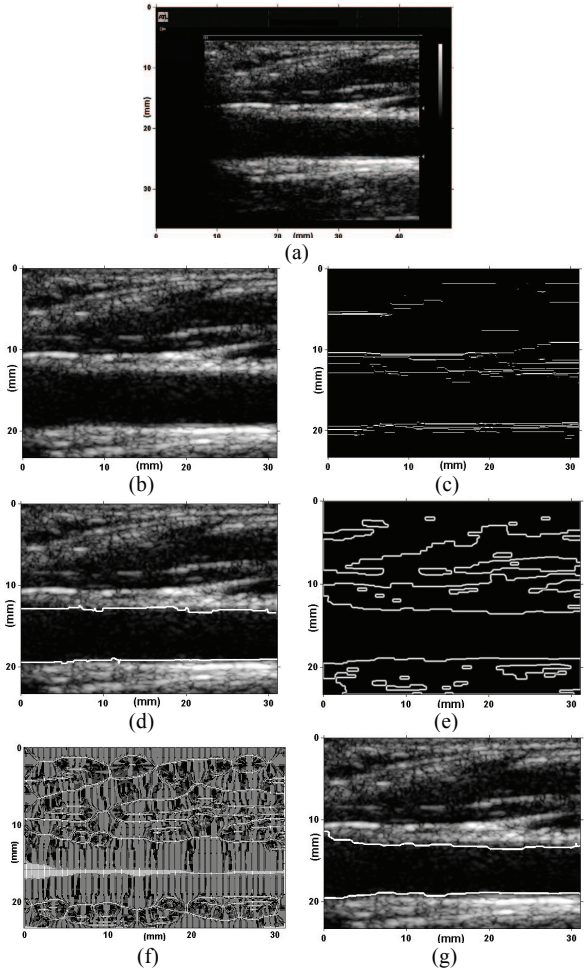


Fig.2 Example of the application of each step of the proposed method (a) original image, (b) reduced image after ROI selection, (c) wavelet-based multiscale edge detection, (d) initial arterial wall estimation, (e) image edge map, (f) GVF field and (g) final contour.

β=0 allows the snake to bend, and thus to detect the random shape of the arterial wall.

The presence of artifacts, i.e small edge segments and/or edge segments inside the lumen, in the investigated images was addressed at the post-processing step of the edge detection stage of the methodology. Such artifacts were removed by applying constraints on the length and the vertical distance of the edge segments during the edge tracing and edge linking process.

It should be noted that the slightly increased computational cost is mainly due to the decomposition and reconstruction procedure, and is directly proportional to the number of scales selected.

5. CONCLUSION

In this paper a new, user-independent and accurate method was developed, to segment ultrasound images of longitudinal sections of the carotid artery. The method is based on multiscale analysis to determine the initial contour of the arterial wall boundary, which is then deformed using GVF snakes. The method will be further evaluated on larger datasets, including images of atherosclerotic vessels.

Table 1 Average values (±std) of sensitivity, specificity and accuracy of the suggested method

	Sensitivity	Specificity	Accuracy
Diastole	0.972 ± 0.006	0.992 ± 0.002	0.987 ± 0.001
Systole	0.976 ± 0.009	0.993 ± 0.002	0.988 ± 0.006

6. REFERENCES

[1] R.S. Reneman, and A.P.G. Hoeks, "Noninvasive vascular ultrasound: an asset in vascular medicine," *Cardiovasc Res* vol. 45, no. 1, 27-35, Jan. 2000.

[2] I. Wendelhag, Q. Liang, T. Gustavsson, and J. Wikstrand, "A new automated computerized analyzing system simplifies reading and reduces the variability in ultrasound measurement of intima media thickness," *Stroke*, vol. 28, no. 2, pp. 2195–2200, Nov. 1997.

[3] S. Golemati, J. Stoitsis, E.G. Sifakis, T. Balkizas, and K.S. Nikita, "Using the Hough transform to segment ultrasound images of longitudinal and transverse sections of the carotid artery," *Ultrasound Med Biol*, vol. 33, no.12, pp. 1918–1932, Dec. 2007.

[4] A.I. Matsakou, S. Golemati, J. Stoitsis, and K.S. Nikita, "Automated detection of the carotid artery wall in longitudinal B-mode ultrasound images using active contours initialized by the Hough transform," *Conf Proc IEEE Eng Med Biol Soc*, vol. 2011, pp. 571-574, Aug. 2011.

[5] R. Rocha, A. Campilho, J. Silva, E. Azevedo, and R. Santos, "Segmentation of the carotid intima-media region in B-mode ultrasound images," *Image Vision Comput*, vol. 28, no. 4, pp. 614-625, Apr. 2010.

[6] F. Molinari, K. M. Meiburger, G. Zeng, A. Nicolaides, and J. S. Suri, "CAUDLES-EF: carotid automated ultrasound double line extraction system using edge flow," *J Digit Imag*, vol. 24, no. 6, pp. 1059–1077, Dec. 2011.

[7] S. Delsanto, F. Molinari, and P. Giustetto, "Characterization of a completely user-independent algorithm for carotid artery segmentation in 2-D ultrasound images," *IEEE Trans Instrum Meas*, vol. 56, no. 4, pp. 1265-1274, Aug. 2007.

[8] F. Molinari, G. Zeng, and J.S. Suri, "Intima-media thickness: setting a standard for a completely automated method of ultrasound measurement," *IEEE Trans Ultrason Ferroelectr Freq Control*, vol. 57, no. 5, pp. 1112-24, May 2010.

[9] N. N. Tsiaparas, S. Golemati, I. Andreadis, J. S. Stoitsis, I. Valavanis, and K. S. Nikita, "Comparison of multiresolution features for texture classification of carotid atherosclerosis from B-mode ultrasound," *IEEE Trans Inf Technol Biomed*, vol. 15, no 1, pp. 130-137, Jan. 2011.

[10] B. Keserci and H. Yoshida, "Computerized detection of pulmonary nodules in chest radiographs based on morphological features and wavelet snake model," *Med Image Anal*, vol. 6, no. 4, pp. 431–447, Dec. 2002.

[11] S. Mallat, S. Zhong, "Characterization of signals from multiscale edges," *IEEE Trans Pattern Anal Machine Intell,* vol. 14, no. 7, pp. 710–732, Jul. 1992.

[12] C. Xu and J.L. Prince, "Snakes, shapes and gradient vector flow," *IEEE Trans Image Process*, vol. 7, no. 3, pp. 359–369, Mar. 1998.

[13] S. Lobregt and M.A. Viergever, "A discrete dynamic contour model," *IEEE Trans Med Imag*, vol. 14, no. 1, pp. 12–24, Mar. 1995.

[14] C. P Loizou, C. Pattichis, M. Pantziaris, A. Nicolaides, "Performance evaluation of active contour models for carotid plaque segmentation," *Proc EMBEC 2005*, vol. 11, no. 1, pp. 1727–1983, Nov. 2005.